

Combined atomic force microscope and acoustic wave devices: Application to electrodeposition

J.-M. Friedt,^{a)} L. Francis, K.-H. Choi, F. Frederix, and A. Campitelli
IMEC, MCP/BIO, Kapeldreef 75, 3001 Leuven, Belgium

(Received 11 October 2002; accepted 7 April 2003)

We present a combination of acoustic wave based sensors with scanning probe microscopy as a tool for better understanding the interaction of the former with the surrounding viscous medium when used for detection of analytes in liquids. Simultaneous analysis of the gold coated sensing surface with an atomic force microscope and monitoring changes in the acoustic propagation properties during copper electrodeposition provides a mean of correlating observations on the nanometer and millimeter scales. We find that the frequency shift of the quartz crystal microbalance is predominantly attributed to viscous effects in the lower mass range (below $1 \mu\text{g}/\text{cm}^2$ copper electrodeposition) and only becomes representative of the added rigid mass in the higher mass range. We observe that the sensitivity of surface acoustic wave Love-mode devices appears constant over the whole mass range analyzed ($0.5\text{--}10 \mu\text{g}/\text{cm}^2$), indicating a rigid layer interaction leading to a frequency shift representative of the deposited mass. © 2003 American Vacuum Society. [DOI: 10.1116/1.1579014]

I. INTRODUCTION

Our aim is to better understand the sensing mechanism of acoustic wave based sensors used in liquid media more specifically for biosensors purposes. Several authors have shown discrepancies between the mass of an electrodeposited metal when comparing the frequency shifts monitored on acoustic sensors and by measuring the current flowing through the potentiostat.^{1,2} Similar discrepancies have been observed for biosensors applications where the added protein layer is viscous and traps water.^{3–6}

In order to be able to monitor surface characteristics at the micrometer and nanometer scales during adsorption reactions, we have combined an atomic force microscope (AFM) with two kinds of acoustic wave devices: quartz crystal microbalance (QCM)⁷ and Love mode surface acoustic wave (SAW) delay lines.⁸ We have focused our analysis on acoustic wave interactions with the surrounding liquid as a function of surface topography by monitoring electrochemical deposition of metals. Such electrodepositions of various metals allow fast reproducible and reversible reactions to occur on the surface, and provide an independent measurement of the mass deposited on the working electrode. Hence, our combination of instruments focuses on using simultaneously acoustic wave sensors, scanning probe microscopy, and electrodeposition, while the sensing area of the acoustic wave device is also used as the working electrode of the electrochemical setup.

II. AFM–QCM INTERACTIONS AND INFLUENCE OF A VISCOUS FLUID

We have first modeled the QCM–AFM interactions in order to better understand the limitations of the combination.⁹ Finite element analysis shows that a QCM

generates longitudinal acoustic waves in the liquid due to the finite size of the electrodes. These longitudinal waves propagate in the liquid and are reflected on the AFM cantilever holder, thus generating standing wave patterns which disturb the resonance frequency of the QCM. On the other hand, the in-plane vibration amplitude in liquid of the QCM is in the nanometer range and AFM resolution is thus not decreased by this 3–5 nm (peak to peak) rough vibrating surface. We can consider that the two instruments, AFM and QCM, do not interfere with each other during normal use when the AFM vertical displacement range is in the hundreds of nanometers and the lateral resolution required is larger than 3 nm. Our experiment lies within these experimental constraints since the crystals we grow on the Au electrode are several tens of nanometers high.

In all cases the experimental procedure for copper electrodeposition on a gold working electrode consists of depositing about $60 \mu\text{l}$ of electrolyte solution including 10^{-2} M $\text{CuSO}_4 + 10^{-2}$ M H_2SO_4 . The electrolyte for silver electrodeposition is made of 10 mM AgNO_3 , 0.5 M KNO_3 , and 0.1 M HNO_3 . The counter electrode is made of a 99.99% pure 0.25-mm-diam Pt wire and the pseudoreference electrode is a 99.98+% pure copper 1-mm-diam wire (as provided by Goodfellow, Huntington, UK) for copper deposition, or a 0.25-mm-diam silver wire during silver electrodeposition. The AFM is a commercial unit (PicoScan, Molecular Imaging, USA) and the resonance frequencies up to the seventh overtone (overtones 1, 3, 5, and 7 at frequencies ranging from 4.7 to 32.9 MHz) of the QCM are simultaneously monitored using the electronics provided by QSense-AB (Göteborg, Sweden) to which a lab-made liquid cell compatible with the AFM was connected. The electrolyte was static in the liquid cell. This setup furthermore allows the measurement of the dissipation of the QCM, defined as the inverse of the quality factor.

By electrodepositing various metals (Cu and Ag) on the

^{a)}Electronic mail: friedtj@imec.be

Au sensing electrode of the QCM while scanning the topography of the surface with the AFM, we were able to relate the dissipation and the ratio of the frequency shift of the first three overtones of the QCM to the overtone number with the roughness of the electrode surface. Indeed, while a flat layer deposited on a flat electrode acts as a rigid layer following the Sauerbrey relation,⁷ a rough surface interacts with the surrounding viscous liquid. Assuming a liquid layer of thickness δ moves with the QCM surface and adds its mass to that of the resonator, where δ is for a Newtonian fluid

$$\delta = \sqrt{\frac{\eta_l}{\pi f_n \rho_l}}, \quad (1)$$

where η_l and ρ_l are, respectively, the dynamic viscosity and density of the liquid (for water, these constants are numerically equal to $0.01 \text{ g cm}^{-1} \text{ s}^{-1}$ and 1 g cm^{-3}), f_n being the resonance frequency of the n th overtone in liquid, we obtain a proportionality relationship between the frequency variation Δf_n of the n th overtone as $\Delta f_n / \sqrt{n}$ and the added mass instead of $\Delta f_n / n$ for a rigid layer. Indeed, assuming that during surface roughening due to large crystal electrochemical growth the factor limiting viscous interaction is the penetration depth of the SAW in the liquid (which is the case when the crystal height becomes of the same order of magnitude as δ), then $\delta \propto 1/\sqrt{n}$ and $\Delta f_n \propto n/\sqrt{n} = \sqrt{n}$ as seen by replacing the rigid mass term in the Sauerbrey equation by the viscous acoustic wave penetration depth (the mass of surrounding liquid interacting with the surface being $\rho_l \delta A$, where A is the sensing electrode area).

The viscous interaction between the vibrating surface and the viscous fluid can thus be identified by two methods: by monitoring the dissipation which increases with increasing viscous interaction with the surrounding liquid, and by measuring the frequency shift of the overtones. The frequency shift Δf_n of n th overtone ($n \in \{1, 3, 5, 7\}$) will evolve with a scaling law $\Delta f_n / n = \text{constant}$ when a rigid layer (negligible viscous interaction with the surrounding liquid compared to the rigid layer mass contribution) is deposited on the QCM, while the scaling law becomes $\Delta f_n / \sqrt{n} = \text{constant}$ when the viscous interaction is predominant. These two behaviors have been observed during, respectively, rough copper electrodeposition and smooth silver electrodeposition. In the former case, 200 nm high copper crystals, as observed by *in situ* AFM imaging, grow on the originally (before electrodeposition) 3 nm peak to peak rough gold electrode, leading to a viscous liquid type interaction. In the latter, 50 nm high silver crystals, as observed by *in situ* AFM imaging, grow on the originally 3 nm peak to peak rough gold electrode, leading to a rigid mass type interaction.

III. SAW DEVICES INTERACTIONS WITH A VISCOUS FLUID

SAW devices, like QCMs, are based on the propagation of a shear wave generated by an oscillating electrical field in a piezoelectric material (quartz or lithium tantalate in our case).¹⁰ As opposed to the QCM where the wave vector of the propagating acoustic field is oriented toward the bulk of

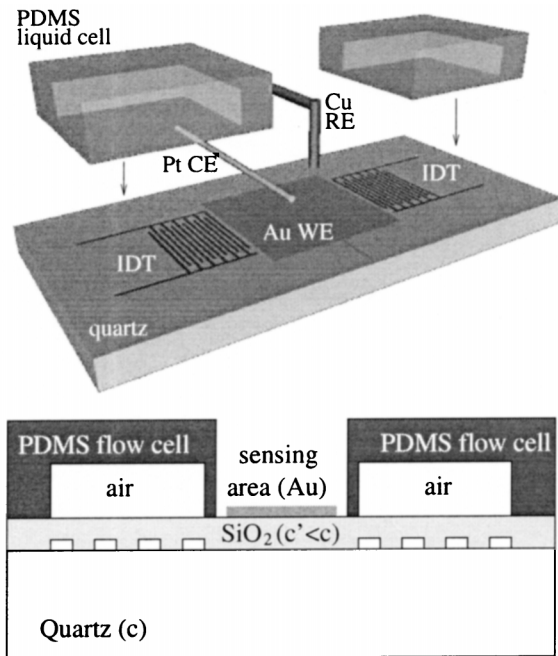


Fig. 1. Experimental setup using a Love mode device: the main issue is to avoid the liquid from reaching the IDEs while reducing insertion losses due to the liquid cell to a minimum. c and c' are the velocity of the shear acoustic wave in quartz and silicon oxide, respectively.

the piezoelectric material, the wave vector of an acoustic field in a SAW device is parallel to the sensing surface and normal to the conducting interdigitated fingers patterned on the surface for generating the acoustic wave (Fig. 1).

When a quartz substrate is patterned with interdigitated electrodes (IDEs) to which an oscillating voltage is applied, the acoustic wave generated is called the surface skimming bulk wave (SSBW). Its mass sensitivity is theoretically predicted to be about the same as that of the QCM, although the wavelength is much smaller ($\lambda = 40 \mu\text{m}$ in our case) to keep the size of the device reasonable, and hence the resonance frequency is much higher (125 MHz in our case).

The sensitivity of SSBW devices can be greatly improved by concentrating the acoustic energy close to the sensing surface. This result is achieved by depositing a thin additional layer, on the order of $\lambda/10$ thickness for a good sensitivity,¹¹ on top of the sensing surface of the quartz wafer: the requirement is for the material used in this additional layer to have an acoustic velocity lower than that of the bulk piezoelectric material. In our case we have deposited, using plasma enhanced chemical vapor deposition, various thicknesses ranging from $\lambda/30$ to $\lambda/20$ of silicon dioxide (SiO_2) whose velocity is assumed to be 2850 m/s,¹² while the velocity of the SSBW in ST quartz propagating normal to the X axis is 5060 m/s.¹² Furthermore, insertion losses are greatly reduced by this energy confinement mechanism, allowing for much simpler electronic circuitry for closed phase locked loop (PLL) operation.

One advantage of SAW devices over the QCM from an instrumentation point of view is that the sensing area is not used as an electrode: while the sensing area of the QCM is a

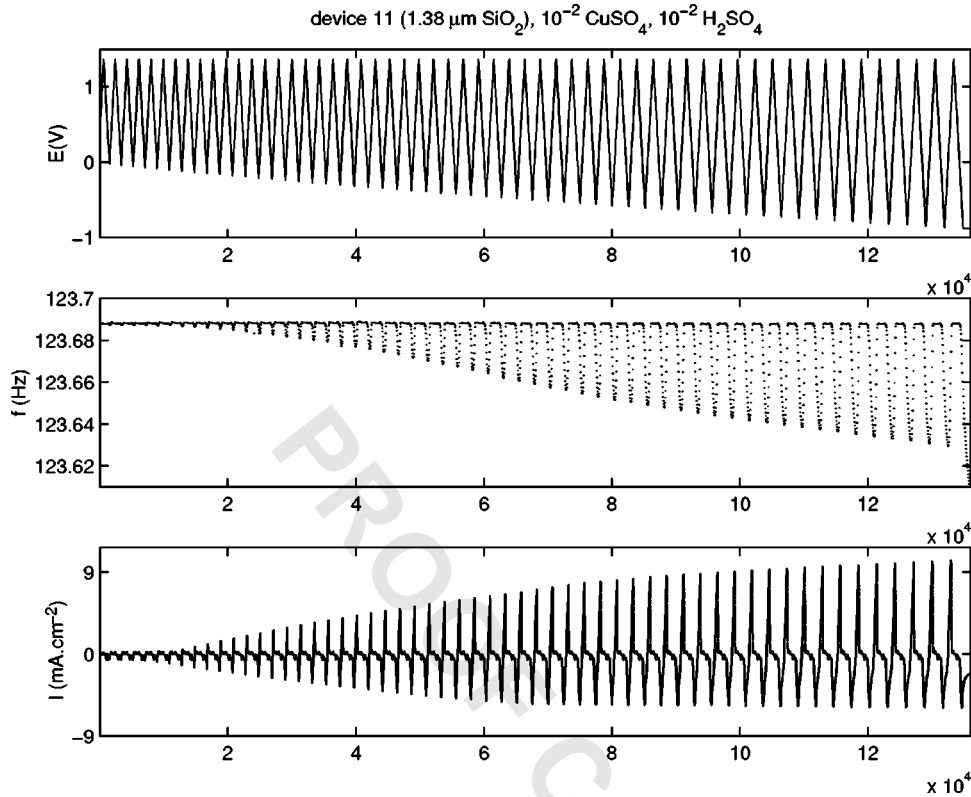


FIG. 2. Example of a raw measurement used for obtaining the sensitivity as a function of deposited mass: (top) applied voltage; (middle) frequency shift; and (bottom) current monitored during electrodeposition (working electrode area: $3.5 \times 3.2 \text{ mm}^2$). Abscissa depict time in arbitrary units.

grounded electrode, the sensing area of the SAW device is open, eventually coated with gold. No additional electrical decoupling of the high frequency signal and of the dc potential is necessary (as was the case in the QCM) for using the mass sensitive region as the working electrode: this area is not used for generating the acoustic wave and can thus be directly connected to the potentiostat.

A. Sensitivity measurements

Using a similar setup as described previously (Sec. II) but by replacing the commercial potentiostat by a simpler lab built version,¹³ we were able to automate the electrodeposition of a variable mass of metal on the sensing area of the SAW devices. The algorithm used for calculating the electrodeposited mass is the following: for each cyclic voltammetry cycle, the maximum and minimum of the oscillation frequency of the acoustic device is monitored (1200 baud RS232 communication from a HP 53132A frequency counter, gate time: 0.1 s) and provide, respectively, $f_0 \approx 125 \text{ MHz}$ the center oscillation frequency and Δf the frequency shift due to mass deposition (Figs. 2 and 3). At the same time, the internal timer of the IBM-compatible personal computer controlling the experiment is monitored and used to calculate the time during which the current density is below $135 \mu\text{A cm}^{-2}$ (which was chosen as a reliable indication of electrodeposition). The deposited mass is then

$$m_{\text{Cu}} = \frac{\sum_j I_j \times \delta t}{N \times e} \times \frac{M_{\text{Cu}}}{n_e},$$

where $\sum_j I_j \times \delta t$ is the number of charges transferred during the electrodeposition process ($\sum_j I_j$ is the sum of the electri-

cal current measurements, δt is the time interval between two current measurements), $N \times e = 96\,440 \text{ C}$ is the charge of one mole of electrons, $M_{\text{Cu}} = 63.5 \text{ g/mol}$ is the molar weight of copper, and $n_e = 2$ is the number of electrons transferred during copper reduction.

We define the sensing area A as the area of the working electrode, i.e., the open area of the liquid cell which completely covers the gold coated region in the center of the SAW device. Although this conducting region extends further than the 3 mm aperture of the fingers of the SAW IDEs, we use the full 3.5 mm width of the opening of the flow cell in our definition of A as prompted by the original derivation of the QCM sensitivity by Sauerbrey: the mass Δm is deposited on the whole working electrode, whether or not in the acoustic path. This additional mass leads to an equivalent additional thickness $\Delta m / (\rho A)$, where ρ is the density of the additional layer assumed to be close to the density of the piezoelectric material in which the acoustic wave is generated. This equivalent additional thickness is the source of the observed frequency shift. This definition of the area used in calculating the sensitivity¹¹ differs from some of the definitions proposed in some of the literature.^{14,15} For example our sensitivity $S = (\Delta f / f_0) \times (A / \Delta m)$ (in g/cm^2) estimate relates to that, $S' = \Delta f / \Delta m$ (in Hz/ng) provided in Ref. 15 by: $S' = S \times f'_0 / A' \times 10^9$, where A' is the area reported in Ref. 15 ($0.3 \times 0.3 \text{ cm}^2$) and f'_0 is the center frequency reported in that same reference ($f'_0 \approx 110 \text{ MHz}$). Numerical application shows that $S' = S \times 0.8$. The results reported here are thus in close agreement to those reported in Ref. 15. Our definition of A is half that of Ref. 14 in which half the width of the IDTs is included.

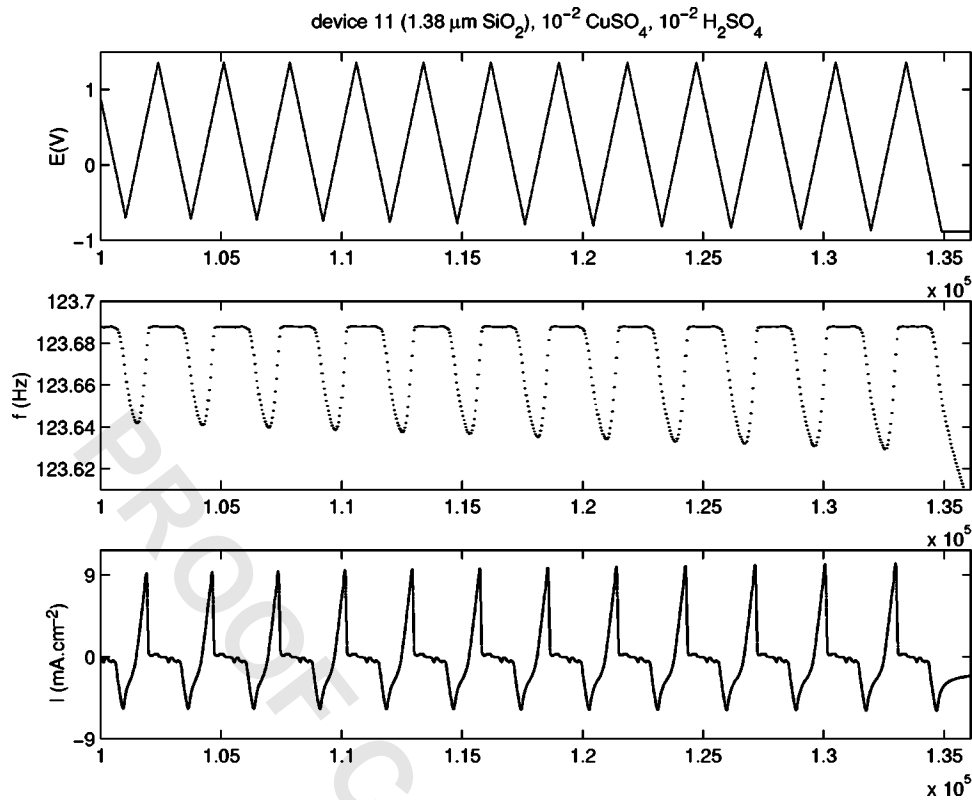


FIG. 3. Zoom of the graph shown in Fig. 2. The negative current is visible when the voltage becomes negative (potential vs the Cu/Cu^{2+} pseudoreference electrode), and the minimum of the frequency is located at the point where the current crosses the 0 A line with a positive slope. Abscissa depict time in arbitrary units.

Thanks to the independent estimate of the deposited mass by measuring the current flowing through the electrochemistry cell, we were able to calculate the experimental sensitivity $S = (\Delta f \times A) / f_0 \Delta m$ (here $A = 3.2 \times 3.5 \text{ mm}^2$).

We observe that a minimum mass must be deposited before the sensitivity reaches a stable asymptotic value compatible with theoretically predicted sensitivity ratios.¹⁶ However, we have identified the drop in sensitivity for lower deposited masses (less than 300 ng on the $3.2 \times 3.5 \text{ mm}^2$ sensing area of our devices) to be an artifact introduced by the current measuring circuit in our potentiostat. Indeed, if we assume the current to voltage conversion circuitry to be subject to leakage current and offset, we introduce a constant offset current measured at the output of the potentiostat. Hence, while the electrochemically deposited mass is M_{Cu} , the mass deduced from the potentiostat reading is $\Delta M = M_{\text{Cu}} + M_{\text{leak}}$, where M_{leak} the mass due to the current measurement error is

$$M_{\text{leak}} = \frac{I_{\text{leak}} \times T}{N \times e} \frac{M_{\text{Cu}}}{n_e}$$

I_{leak} is the offset in current measurement (assumed constant during the measurement) and T the duration of an electrodeposition step. Assuming the frequency shift Δf of the SAW device to be solely due to the deposited mass M_{Cu} through the constant theoretical sensitivity S_{th} , we obtain $\Delta f = (S \times f_0 \times M_{\text{Cu}}) / A$. We finally observe an experimental sensitivity

$$S = \frac{\Delta f}{f_0} \frac{A}{\Delta m} = S_{\text{th}} \frac{M_{\text{Cu}}}{M_{\text{Cu}} + M_{\text{leak}}}$$

The plot displayed in Fig. 4 displays S as a function of ΔM which we have just shown to be $S_{\text{th}} M_{\text{Cu}} / (M_{\text{Cu}} + M_{\text{leak}})$ as a function of $M_{\text{Cu}} + M_{\text{leak}}$. An excellent fit between the experimental curve and this model can be obtained by using the asymptotic value of S for S_{th} as observed for masses greater than $4 \mu\text{g}/\text{cm}^2$ (where $M_{\text{Cu}} \gg M_{\text{leak}}$).

B. AFM combination

In order to get a better understanding of the phenomena occurring on the sensing area, we included the SAW device on the sample stage of an AFM. The major issue in this combination is in the engineering of the liquid cell protecting the IDEs from contact with the liquid (which, by changing the impedance between the interdigitated electrodes, greatly reduces the intensity of the acoustic field generated) while still allowing for the AFM cantilever to reach the sensing surface. The molded polydimethylsiloxane (PDMS) (Sylgard 184 as provided by Dow Corning, Germany—processed by 24 h curing at room temperature in a Teflon mold) flow cell was designed to prevent liquid from reaching the IDEs while minimizing the area of polymer covering the acoustic sensing path: the width of the PDMS lip covering the acoustic path was reduced to $100 \mu\text{m}$ which is the minimum dimen-

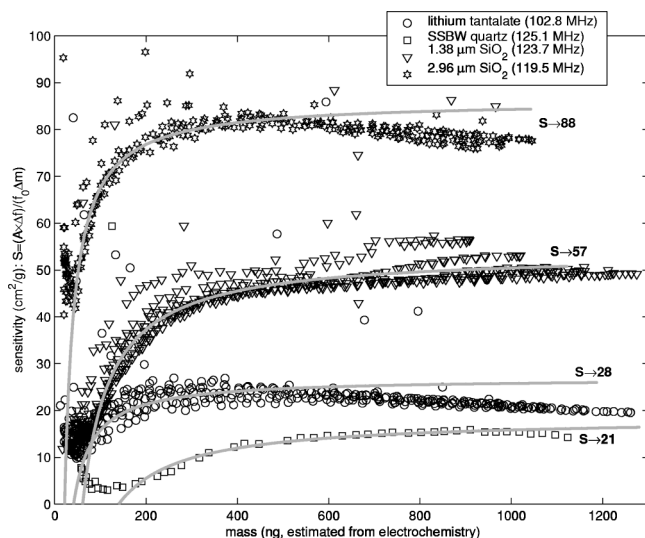


Fig. 4. Sensitivity estimates as calculated from the mass derived from the current measured to flow through the potentiostat during one cyclic voltammetry cycle and the corresponding frequency shift observed on various types of acoustic wave devices. The curves were swept in both directions (increasing and decreasing masses) and no visible hysteresis effect is visible. The gray lines are fits using the model, including an offset in the current measurement, and leading to an asymptotic sensitivity as indicated at the right-most part of each curve.

sion that could be reached when fabricating the mold using classical mechanical milling tools. The open sensing area of the working electrode was then $5 \times 5 \text{ mm}^2$.

An analytical analysis¹⁰ of the displacement (in the plane of the surface on which the acoustic wave propagates, parallel to the interdigitated fingers) of the ST-cut quartz surface due to an applied potential $\Delta\Phi$ between two infinite electrodes shows that the proportionality coefficient is about $10^{-12} - 10^{-11} \text{ m/V}$. Hence, when $\Delta\Phi \approx 5 \text{ V}$, the maximum displacement is in the tens of picometers range, much below the AFM resolution. Since an SSBW mode device is not oscillating in a resonant configuration, we observe that the surface displacement is not dependent on the oscillating frequency and a dc analysis can be extended to an oscillating condition.

Results of an AFM combination with SSBW and Love mode devices operated, respectively, in open loop (monitoring of the phase and insertion loss at a given frequency using an HP 4396A network analyzer) or closed loop configurations (PLL based on one MiniCircuits MAR8 or two MiniCircuits MAR1 amplifiers) are displayed in Fig. 5. The horizontal axis of the AFM images (slow scanning direction) can be interpreted as a time axis representative of the evolution during an electrodeposition cycle of the surface topog-

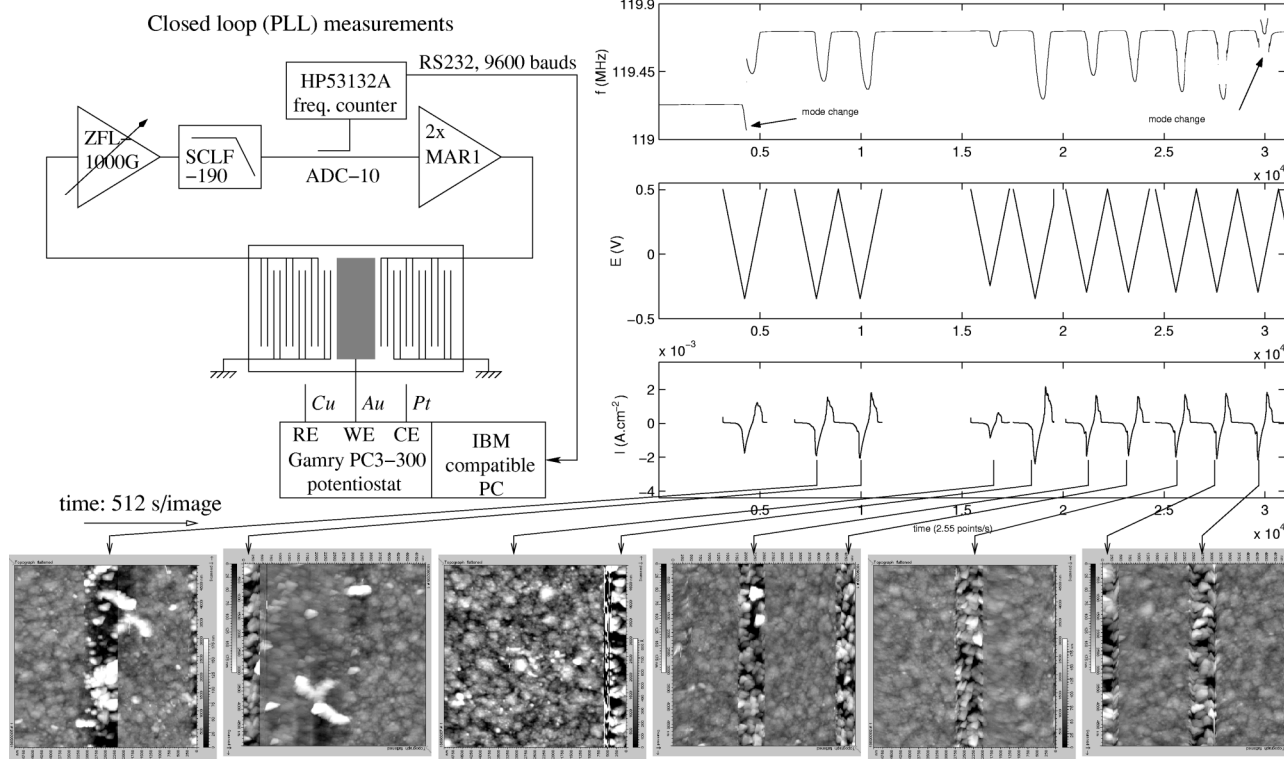


Fig. 5. AFM combination with the SAW device running in a closed loop configuration: monitoring simultaneously the PLL oscillation frequency around 119.5 MHz; cyclic voltammetry voltage and current density; and AFM topography. All images cover a $5 \times 5 \mu\text{m}^2$ area. All components references in the PLL circuit schematic refer to devices from MiniCircuits (New York). The electrolyte used during this experiment is $10^{-2} \text{ M CuSO}_4 + 10^{-2} \text{ M H}_2\text{SO}_4$. Working electrode area: $5 \times 5 \text{ mm}^2$.

raphy. The latter is seen in the vertical axis of these images, which is also the fast scanning direction. The SAW frequency measurements have been synchronized with current and potential information from the potentiostat and arrows indicate the correspondence between each electrodeposition step and the topography change of the surface as observed on the AFM images. Surface roughening due to copper crystals growth (initial surface roughness is 5 nm peak to peak while the copper crystals are several tens of nanometers high) is visible on the AFM topography images, while the contrast increases during electrodeposition cycles is an artifact of the AFM image processing software which automatically compensates for variations in each average line value. Hence, the background appears darker—lower in terms of topography—as a result of the software compensation for the height increase during copper crystal growth.

C. Interpretations

Our sensitivity estimates are lower than previous reports for similar Love mode devices.¹⁶ We explain this discrepancy by the different sensitivity measurement methods: while previous estimates were obtained in air or in vacuum by depositing or etching a layer of material using microelectronics techniques,^{14–17} we measure it here in liquid medium. Such measurements seem more reliable when the sensor is to be used in liquid in its final application (biosensors). The good fit between experimental data and a model assuming constant sensitivity of the acoustic wave device means the viscous interaction is not predominant as a cause of the frequency shift when a mass is added on the sensing area: a rigid layer interaction is sufficient to interpret the data.

We have observed that the AFM and Love mode device do not interact except during the AFM cantilever approach phase (data not shown). During that initial step, the AFM cantilever is brought closer to the SAW sensing area, from an initial distance about 70 μm to a final distance of about 5 μm (tip length as provided by the manufacturer). We attribute this frequency increase with decreasing distance to capacitive effects between the nonconducting cantilever holder and the floating potential sensing electrode. Indeed, during this initial stage the working electrode of the potentiostat is not connected and the working electrode is in a high impedance state. The initial approach distance is, however, much greater than any further distance variation during an actual surface

scan during which the working electrode is connected to a low-impedance output, so that no capacitive fluctuation occurs during AFM monitoring of the electrodeposition steps.

The combined AFM/SAW experiment thus leads to results compatible with those obtained in the combined AFM/QCM experiment, with the added advantage in the former setup of increased sensitivity and more accessible sensing electrode.

IV. CONCLUSION

We have here shown how electrodeposition can be efficiently used for measuring the sensitivity parameter of acoustic wave sensors to be used in liquids. We have shown how a combination with the AFM provides better insight into the phenomena happening on the surface by monitoring the electrodeposition at the nanometer scale.

ACKNOWLEDGMENT

Laurent Francis is supported by the Belgian FRIA fund (fonds pour la Formation à la Recherche dans l'Industrie et dans l'Agriculture).

- ¹R. Schumacher, G. Borges, and K. K. Kanazawa, *Surf. Sci. Lett.* **163**, L621 (1985).
- ²R. Schumacher, J. G. Gordon, and O. Melroy, *J. Electroanal. Chem. Interfacial Electrochem.* **216**, 127 (1987).
- ³M. Muratsugu, F. Ohta, Y. Miya, T. Hosokawa, S. Kurosawa, N. Kamo, and H. Ikeda, *Anal. Chem.* **65**, 2933 (1993).
- ⁴F. Höök *et al.*, *Colloids Surf., B* **24**, 155 (2002).
- ⁵M. V. Voinova, M. Johnson, and B. Kasemo, *Biosens. Bioelectron.* **17**, 835 (2002).
- ⁶E. Howe and G. Harding, *Biosens. Bioelectron.* **15**, 641 (2000).
- ⁷A. Janshoff, H.-J. Galla, and C. Steinem, *Angew. Chem., Int. Ed. Engl.* **39**, 4004 (2000).
- ⁸B. Jakoby and M. J. Vellekoop, *IEEE Trans. Ultrason. Ferroelectr. Freq. Control* **45**, 1293 (1998).
- ⁹J.-M. Friedt, K. H. Choi, L. Francis, and A. Campitelli, *Jpn. J. Appl. Phys., Part 1* **41**, 3974 (2002).
- ¹⁰*Acoustic Fields and Waves in Solids*, edited by B. A. Auld (Wiley, New York, 1973), Vol. 1.
- ¹¹G. Kovacs, G. W. Lubking, M. J. Vellekoop, and A. Venema, *Proceedings Ultrasonics Symposium*, 1992, p. 281.
- ¹²Z. Wang and J. D. N. Cheeke, *Appl. Phys. Lett.* **64**, 2940 (1994).
- ¹³M. Deluzarche and É. Zimmerlin, *Bull. Union Physiciens* **96**, 103 (2002).
- ¹⁴J. Du, G. L. Harding, J. A. Ogilvy, P. R. Dencher, and M. Lake, *Sens. Actuators A* **56**, 211 (1996).
- ¹⁵G. L. Harding, *Sens. Actuators A* **88**, 20 (2001).
- ¹⁶J. Du and G. L. Harding, *Sens. Actuators A* **65**, 152 (1998).
- ¹⁷K. K. Zadeh, A. Trinchì, W. Włodarski, and A. Holland, *Sens. Actuators A* **100**, 134 (2002).